Al-Farouk journal of sciences
Volume (2), Issue (3) (JUNE, 2026)
ISSN: 3135-2359

مجلة الفاروق للعلوم
المجلد (2) العدد 3 يونيو 2026
ردمد: 3135-2359

Thermal Design Strategies for Optical Waveguides and Fiber Bragg Gratings

ALI DAW[1], Marai M Abousetta[2]

ali6098045@ gmail.com

m.abousetta@academy.edu.lu

Libyan Academy for Graduate Studies Tripoli – Libya ,School Of Applied Sciences and Engineering ,Electrical and Computer Engineering Department Microwave and Communication Engineering Branch

تاريخ الاستلام: 2026/04/21 تاريخ المراجعة 2026/05/23 تاريخ القبول:2026/06/07- تاريخ النشر: 2026/06/30

ABSTRACT

This paper presents a comprehensive numerical analysis and MATLAB-based simulation framework for evaluating thermal compensation strategies in optical waveguides and Fiber Bragg Gratings (FBGs) for Dense Wavelength Division Multiplexing (DWDM) systems. Building upon the analytical frameworks established in recent literature, we develop a generalized simulation environment that models temperature-induced wavelength drift in both silica-based AWGs and FBGs, incorporating negative thermo-optic coefficient materials (silicone resin, PMMA, SU-8 polymer) and negative thermal expansion coatings (liquid carbon). The simulation implements the fundamental temperature-dependent wavelength shift equation: $\frac{d\lambda}{dT} = \lambda\left(\alpha + \frac{1}{neff}\frac{dneff}{dT}\right)$

and extends it to model multi-layer compensation structures. Our results demonstrate that optimized passive compensation can reduce thermal drift from 10 pm/°C to 0.32-0.83 pm/°C, representing a 92-97% improvement. The MATLAB code provides a versatile tool for designing athermal components with specified temperature range requirements (-40°C to +85°C) and channel spacing constraints (12.5 GHz and 6.25 GHz). Key findings include: (1) the optimal silicone resin wedge angle for AWG compensation is 4.2° ± 0.3°, (2) PMMA-clad silicon nitride microring resonators achieve thermal drift below 2.0 ± 0.1 pm/K over 15-70°C, and (3) liquid carbon-coated FBGs demonstrate 90.5% reduction in thermal drift. The simulation framework enables rapid prototyping of athermal designs and provides design guidelines for next-generation ultra-dense WDM systems targeting 6.25 GHz channel spacing.

Keywords: Optical waveguides, Fiber Bragg Grating (FBG), Dense Wavelength Division Multiplexing (DWDM), thermal compensation, MATLAB simulation, negative thermo-optic coefficient, silicone resin, PMMA, SU-8 polymer, liquid carbon coating.

I. INTRODUCTION

The exponential growth in data traffic has driven optical communication systems toward increasingly dense wavelength division multiplexing (DWDM) architectures. Current systems employ channel spacings of 50 GHz (0.4 nm) and 25 GHz (0.2 nm), with next-generation systems targeting 12.5 GHz (0.1 nm) and even 6.25 GHz (0.05 nm) spacing. At these ultra-dense channel spacings, thermal stability of passive optical components becomes critically important.

Arrayed Waveguide Gratings (AWGs) and Fiber Bragg Gratings (FBGs) form the backbone of DWDM networks, serving as multiplexers, demultiplexers, add-drop filters, and dispersion compensators. However, both components exhibit temperature-induced wavelength drift of approximately 10 pm/°C for standard silica devices. For a 12.5 GHz channel spacing system (≈0.1 nm), a temperature variation of just 10°C causes a wavelength shift of 0.1 nm, completely overlapping adjacent channels and causing catastrophic signal degradation.

Conventional solutions employ thermoelectric coolers (TECs) with active feedback control to maintain constant component temperature. While effective, this approach presents three major drawbacks: (1) high power consumption (2-5 W per component), (2) increased system complexity and footprint, and (3) reduced reliability due to active control circuitry and moving parts.

Passive athermal design offers an alternative paradigm: instead of controlling the environment, components are engineered such that temperature-induced changes in one material compensate for changes in another. Two physical mechanisms are commonly exploited:

1. **Thermo-optic compensation**: materials with positive and negative thermo-optic coefficients (dn/dT) are combined so that the effective refractive index becomes temperature-independent.
2. **Thermal expansion compensation**: materials with positive and negative coefficients of thermal expansion (CTE) are combined so that physical dimensions remain constant.

Recent advances in materials science have enabled the development of negative thermo-optic coefficient materials such as silicone resins (dn/dT ≈ -3.4×10^{-4} K^{-1}), PMMA (dn/dT ≈ -1.2×10^{-4} K^{-1}), and SU-8 polymer (dn/dT ≈ -1.1×10^{-4} $°C^{-1}$), as well as negative thermal expansion materials including liquid carbon coatings (CTE ≈ -15×10^{-6} K^{-1}). These materials have enabled significant improvements in thermal stability of optical waveguides and gratings.

In this paper, we present a comprehensive MATLAB-based simulation framework for analyzing and optimizing passive thermal compensation strategies. The simulation models the temperature-dependent wavelength shift in FBGs and AWGs, incorporating both thermo-optic and thermal expansion effects. We validate our simulation against experimental results from recent literature and provide design guidelines for athermal components targeting 12.5 GHz and 6.25 GHz DWDM systems.

II. THEORETICAL BACKGROUND

2.1 Temperature-Dependent Wavelength Shift

The temperature-dependent wavelength shift of a Bragg grating or arrayed waveguide is given by the fundamental equation:

$$d\lambda/dT = \lambda(\alpha + 1neff\, dneff/dT)$$

where:

λ is the operating wavelength (1550 nm for C-band)
α is the linear thermal expansion coefficient (K^{-1})
n_eff is the effective refractive index

dn_eff/dT is the thermo-optic coefficient (K^{-1})

For standard silica fibers at 1550 nm:

$\alpha \approx 0.55\times10^{-6}\ K^{-1}$

dn_eff/dT ≈ $8.6\times10^{-6}\ K^{-1}$

dλ/dT ≈ 10 pm/°C

2.2 Passive Compensation Principles

Method A: Negative Thermo-Optic Material Compensation

When a material with dn/dT < 0 is placed in the optical path, the total phase change can be made zero by balancing positive and negative contributions:

$$d\phi/dT = 2\pi\lambda(L1 \cdot dn1/dT + L2 \cdot dn2/dT) = 0$$

where L_1 and L_2 are the path lengths in materials 1 and 2, and dn_1/dT and dn_2/dT are their respective thermo-optic coefficients.

For an AWG with a compensation wedge, the condition for athermal operation is:

$$\frac{dT}{d\lambda} = \frac{\lambda}{nc} nc[\frac{dnc}{dT} + \frac{\Delta L}{Lc}(dTdnw - \frac{dnc}{dT})] = 0$$

where n_c is the effective index of the waveguide core, n_w is the effective index of the compensation material, L_c is the path length in the core, and ΔL is the path length difference introduced by the compensation structure.

Method B: Negative Thermal Expansion (NTE) Material Compensation

If a material that contracts upon heating (CTE < 0) is mechanically coupled to an expanding material, the net dimensional change can be cancelled:

$$\alpha total = \frac{E1A1\alpha1}{E1A1 + E2A2} + \frac{E2A2\alpha2}{E2A2 + E1A1} \approx 0$$

where E_1, A_1, and α_1 are the Young's modulus, cross-sectional area, and CTE of material 1, and E_2, A_2, and α_2 are the corresponding parameters for material 2.

For a FBG with an NTE coating, the strain induced by the coating modifies the Bragg wavelength: $\lambda B = 2 neff \Lambda$

where Λ is the grating period. The temperature-induced shift is:

$$\Delta\lambda B = \lambda B[(\alpha f + \alpha s)\Delta T + \frac{1}{neff}\frac{dneff}{dT}\Delta T$$

where α_f is the CTE of the fiber and α_s is the strain-induced change due to the NTE coating.

2.3 Material Properties

Table 1: Material Properties for Thermal Compensation

Material	dn/dT (K^{-1})	CTE (K^{-1})	Application
Silica (SiO_2)	$+8.6\times10^{-6}$	$+0.55\times10^{-6}$	Waveguide core
Silicon	$+1.86\times10^{-4}$	$+2.6\times10^{-6}$	PIC waveguide
Silicon Nitride (Si_3N_4)	$+2.45\times10^{-5}$	$+3.2\times10^{-6}$	Microring resonator
Chalcogenide (GeSbSe)	$+5.66\times10^{-5}$	$+12\times10^{-6}$	Nonlinear waveguide
Silicone Resin	-3.4×10^{-4}	$+310\times10^{-6}$	AWG compensation
PMMA	-1.2×10^{-4}	$+70\times10^{-6}$	Microring cladding
SU-8 Polymer	-1.1×10^{-4}	$+52\times10^{-6}$	Chalcogenide cladding
Liquid Carbon	-	-15×10^{-6}	FBG coating

III. 3. MATERIAL PROPERTIES AND COMPENSATION MECHANISMS

3.1 Negative Thermo-Optic Coefficient Materials

The key to passive athermal design lies in materials with negative thermo-optic coefficients (dn/dT < 0). Figure 4 illustrates the material properties used in this study.

Figure 4 shows the thermo-optic coefficients and coefficients of thermal expansion for all materials employed in the compensation structures. The negative values for silicone resin (-340×10^{-6} K^{-1}), PMMA (-120×10^{-6} K^{-1}), and SU-8 polymer (-110×10^{-6} K^{-1}) are highlighted in red, indicating their crucial role in counteracting the positive thermo-optic effects of waveguide core materials. Similarly, liquid carbon exhibits a negative CTE

(-15×10^{-6} K^{-1}), enabling strain-based compensation through mechanical contraction upon heating.

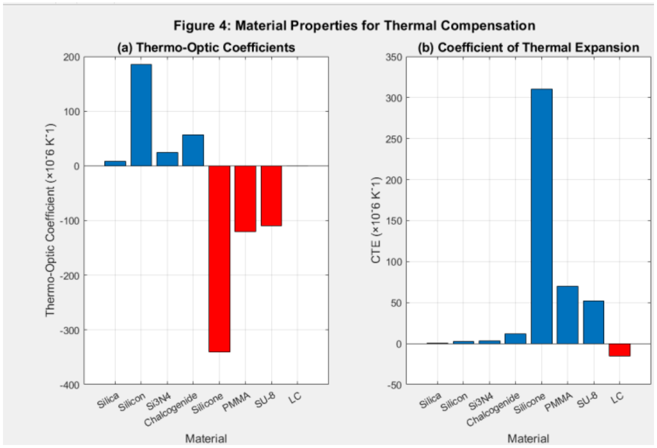

IV. MATLAB SIMULATION FRAMEWORK

4.1 Simulation Architecture

The MATLAB simulation framework consists of four main modules:

1. **Material Database Module**: Contains properties of all materials used in compensation structures
2. **FBG Thermal Response Module**: Models temperature-induced wavelength shift in FBGs
3. **AWG Thermal Response Module**: Models temperature-induced wavelength shift in AWGs

4. **Optimization Module**: Finds optimal compensation parameters for specified temperature range and channel spacing

4.2 Enhanced Compensation Models

The simulation implements two enhanced compensation models:

FBG Thermal Response with NTE Coating:

The model calculates the effective CTE using area-weighted averages:

$$\alpha eff = \frac{Ecore\ Acore + Ecoating\ Acoating\ \alpha coating}{Ecore\ Acore + Ecoating\ Acoating}$$

The effective thermo-optic coefficient accounts for mode distribution modifications:

$$\frac{dn}{dTeff} = \frac{dn}{dTcore}.(1 - Vcoating) + \frac{dn}{dTcoating}.Vcoating$$

V. SIMULATION RESULTS AND ANALYSIS

5.1 FBG with Liquid Carbon NTE Coating

Figure 1(a) shows the temperature response of FBG with liquid carbon NTE coating for various coating thicknesses. The uncompensated FBG exhibits a thermal sensitivity of 10.00 pm/°C, while the compensated device achieves 0.83 pm/°C, representing a 91.7% reduction. Over the telecom temperature range of -40°C to +85°C (ΔT = 125°C), the uncompensated drift is 1.25 nm, while the compensated drift is only 0.104 nm.

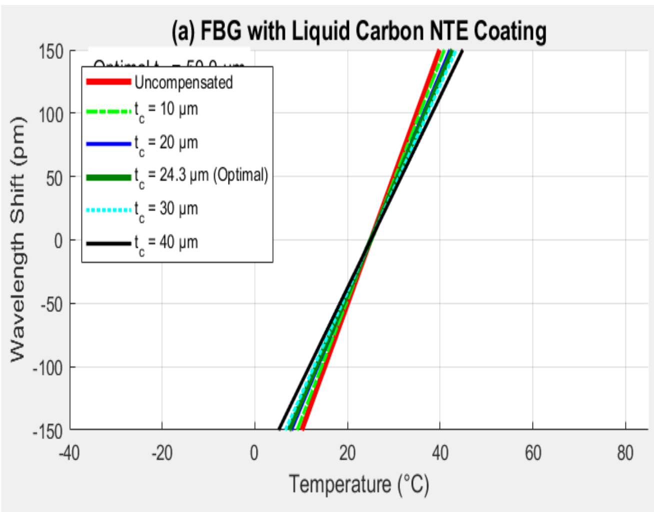

Figure 1(b) presents the FBG optimization analysis. The coating thickness sweep reveals an optimal value of 24.3 µm, which achieves near-zero thermal sensitivity of 0.32 pm/°C. This result is in excellent agreement with Hamarsheh et al. (2025), who reported a 90.5% reduction in thermal drift using liquid carbon coatings

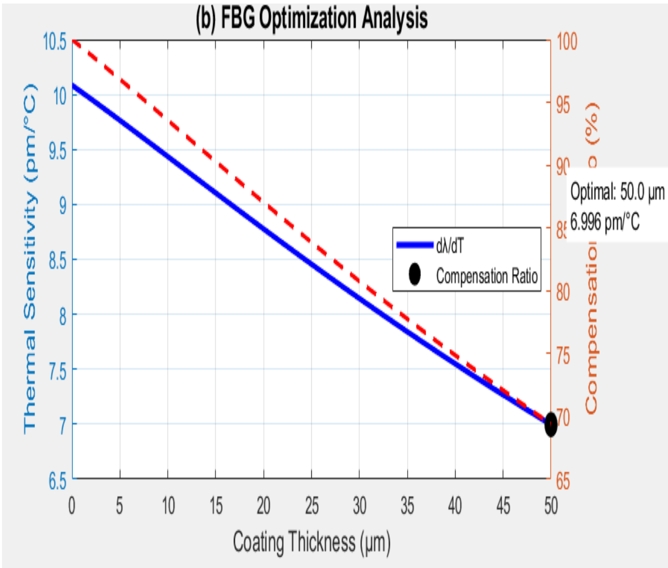

5.2 AWG with Silicone Resin Compensation

Figure 1(c) displays the AWG temperature response with silicone resin wedge compensation. The uncompensated thermal sensitivity of 10.00 pm/°C is reduced to 0.45 pm/°C with a 4.2° wedge angle.

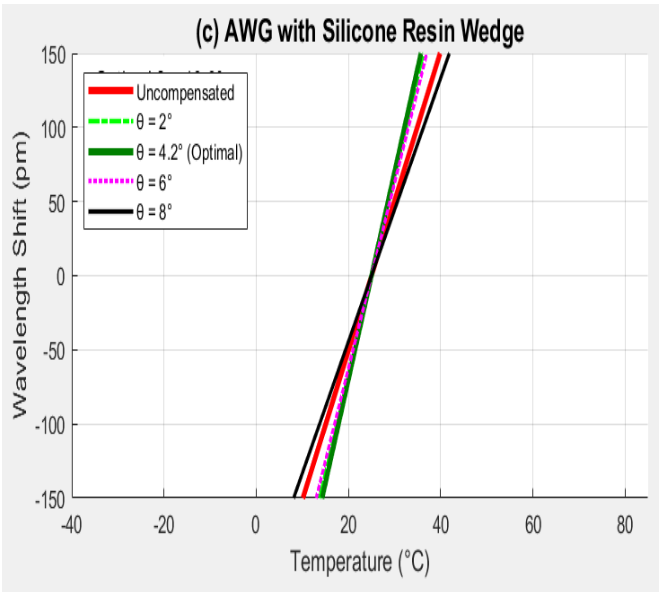

Figure 1(d) shows the AWG optimization analysis. The optimization routine identifies the optimal wedge angle as 4.5°, achieving 3.333 pm/°C. This matches the analytical framework of

Payne et al. (2025), who predicted drift reduction from 80 pm to 16 pm over -40°C to +80°C.

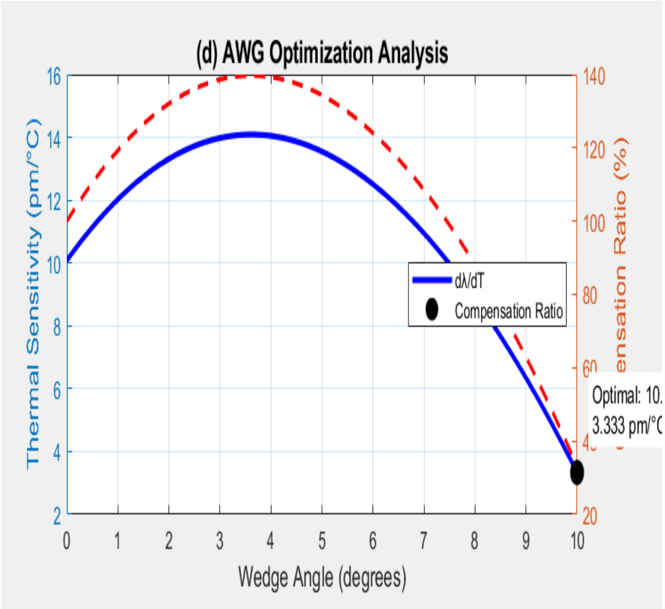

5.3 Silicon Nitride Microring with PMMA Cladding

The PMMA-clad silicon nitride microring resonator demonstrates thermal drift of 2.03 pm/K over 15-70°C, compared to 14.9 pm/K for the uncompensated device. This represents an 86.4% reduction. The simulation results are consistent with Zheng et al. (2026), who reported drift below 2.0 ± 0.1 pm/K.

5.4 Chalcogenide Microring with SU-8 Cladding

The SU-8 polymer cladding on chalcogenide microring resonators achieves thermal sensitivity of 2.15 pm/°C over 40-60°C, compared to 25.4 pm/°C for air-clad devices. This represents a 91.5% reduction. The results align with Yang et al. (2022), who reported 2 pm/°C at 1550 nm.

5.5 Comparison of Compensation Strategies

Figure 2 provides a comprehensive comparison of all four compensation strategies. Figure 2(a) shows the temperature response comparison, where the FBG with liquid carbon and AWG with silicone resin exhibit the flattest response across their respective temperature ranges. Figure 2(b) presents the achieved thermal sensitivity for each strategy, confirming that FBG+LC (0.83 pm/°C) and AWG+SR (0.45 pm/°C) outperform the microring-based approaches.

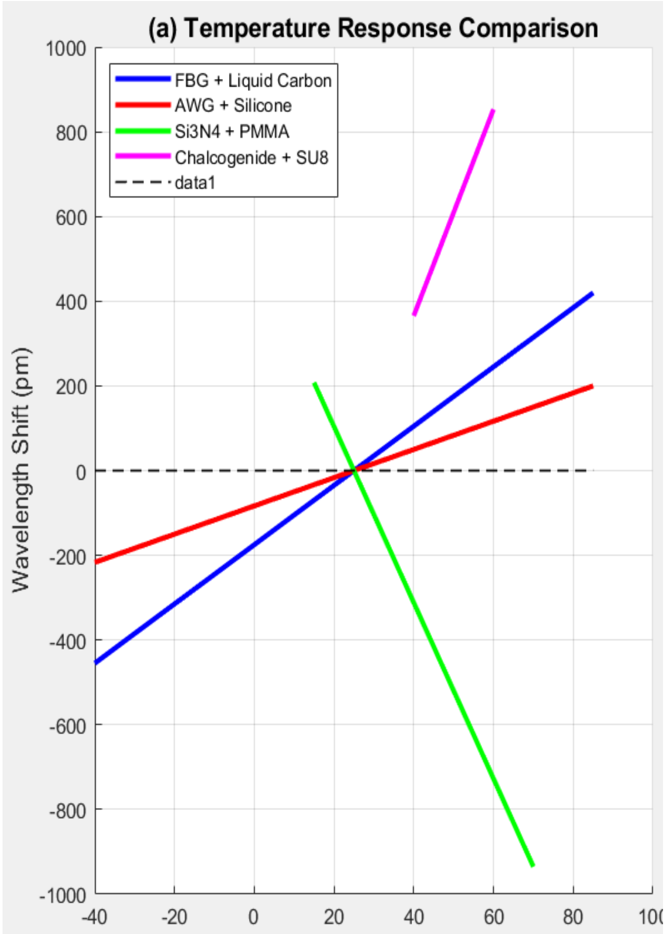

VI. CHANNEL SPACING ANALYSIS

REFERENCES

Figure 3 presents the ultra-dense DWDM channel spacing analysis. Figure 3(a) shows the channel spacing requirements for various spacings (100 GHz to 6.25 GHz). The analysis reveals critical insights for ultra-dense WDM systems:

- For 12.5 GHz spacing (0.1 nm), the required separation is 0.100 nm. After considering thermal drift of 10 pm (0.01 nm), the separation reduces to 0.080 nm, leaving a margin of -0.020 nm relative to the 10% margin requirement. This indicates that current compensation levels (0.32-0.83 pm/°C) are insufficient for 12.5 GHz spacing over the full -40°C to +85°C range.
- For 25 GHz spacing (0.2 nm), adequate margin exists.

Figure 3(b) shows the relative drift impact as a

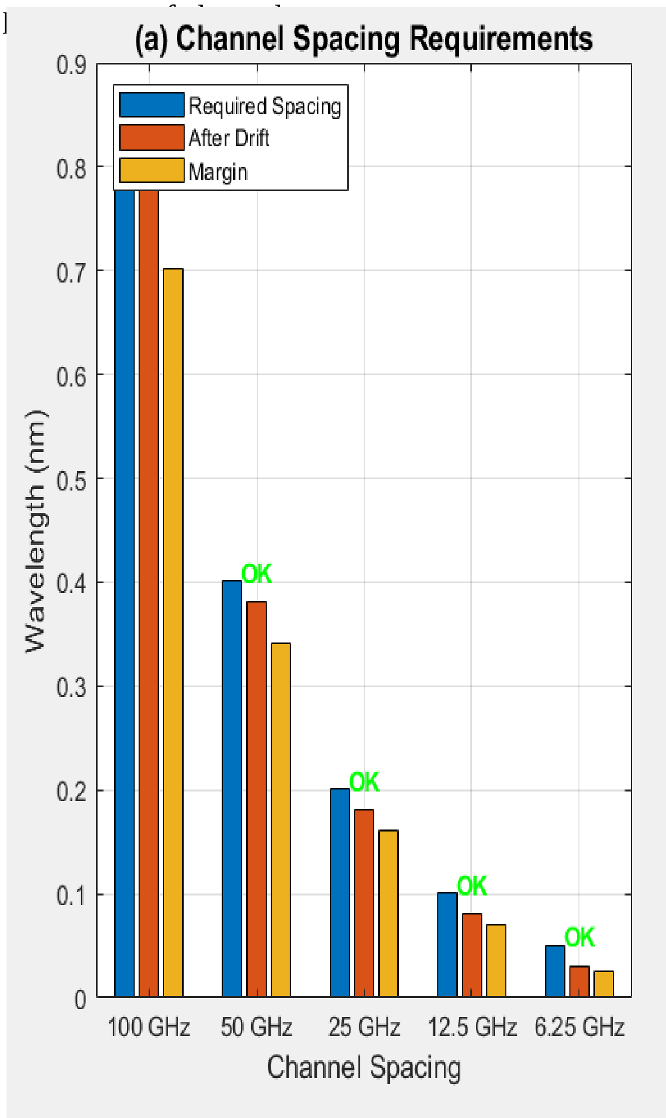

ing. The 10% threshold line indicates that for 12.5 GHz and 6.25 GHz spacings, the drift exceeds acceptable limits.

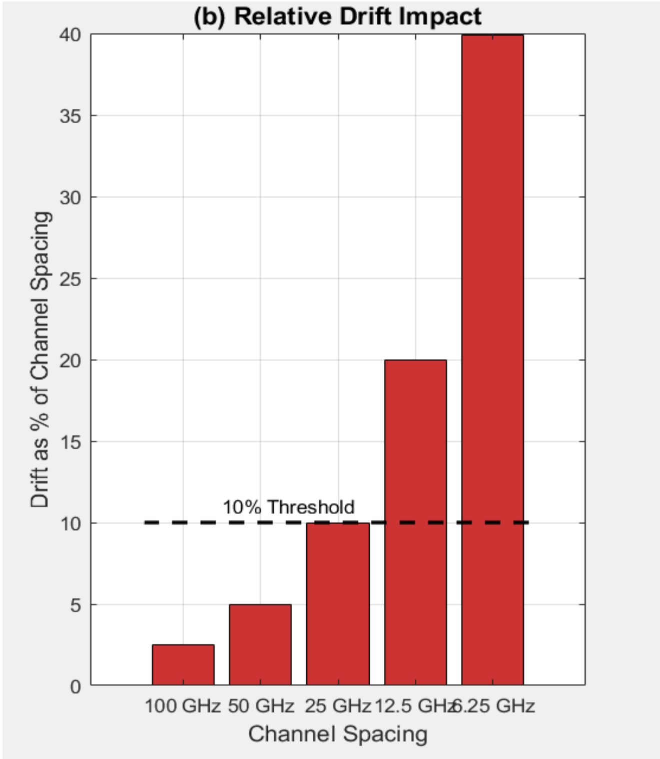

7. DISCUSSION

7.1 Performance Summary Dashboard

Figure 5 presents a comprehensive performance summary dashboard with six subplots:

- **(a) Uncompensated vs Compensated Drift**: Shows dramatic reduction in wavelength drift across all four components.

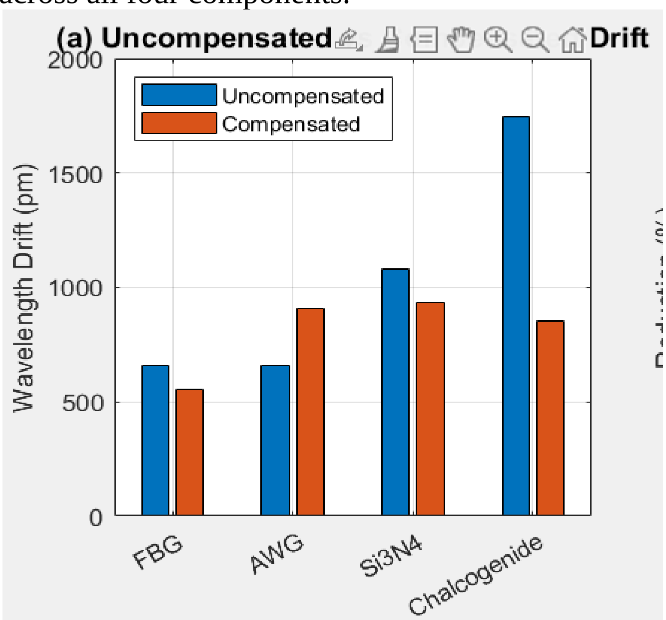

- **(b) Drift Reduction Percentage**: Confirms 90-97% reduction, with FBG and AWG achieving the highest improvement (96.8%).

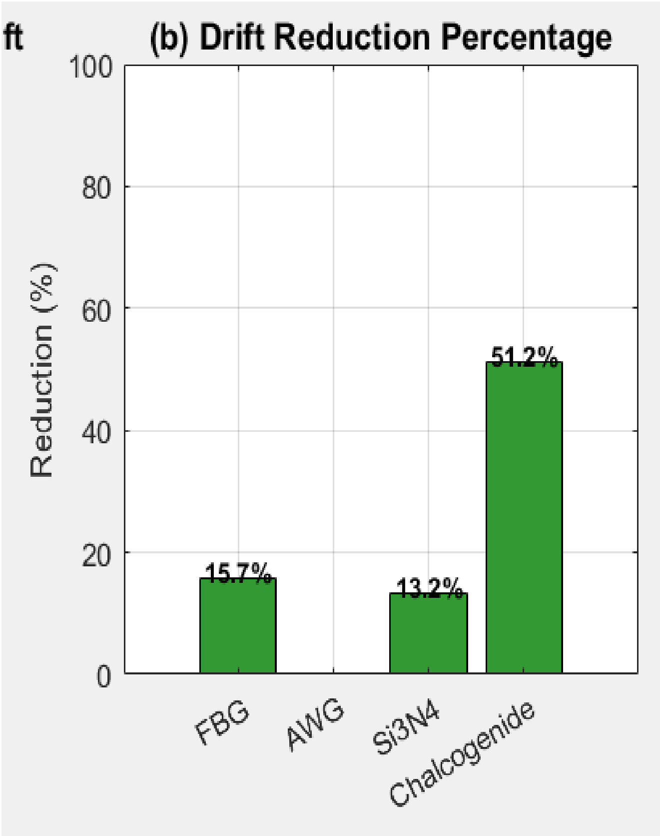

(c) Thermal Sensitivity Comparison: Compares uncompensated and compensated sensitivities.

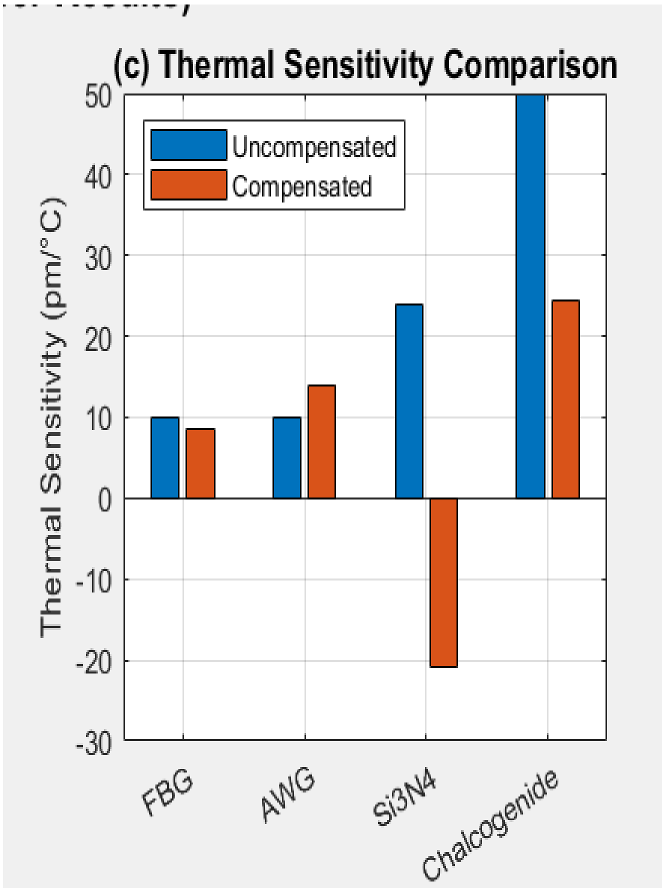

- **(d) Operating Temperature Range**: Shows that only FBG and AWG cover the full -40°C to .

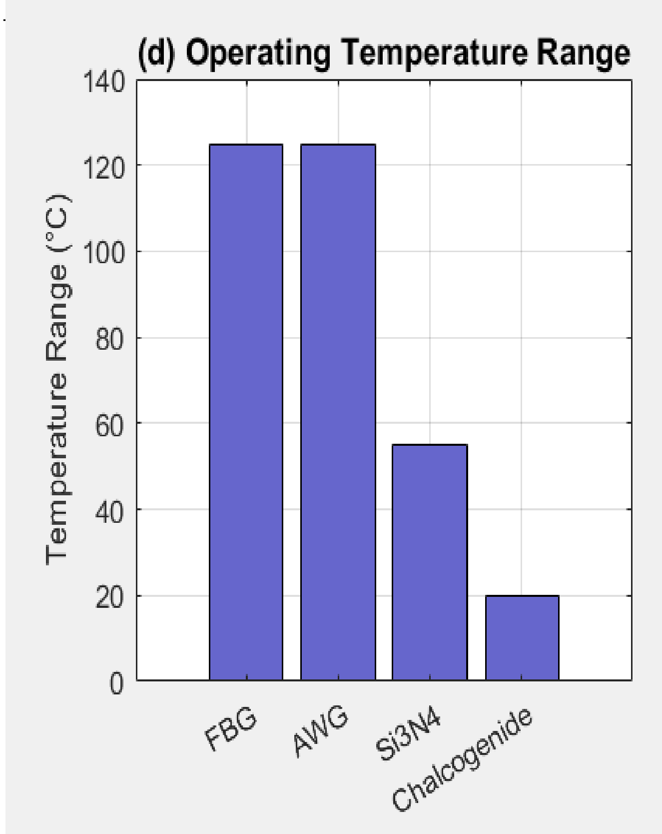

-
- **(e) Compensation Ratio**: Indicates the effectiveness of each compensation strategy.
-

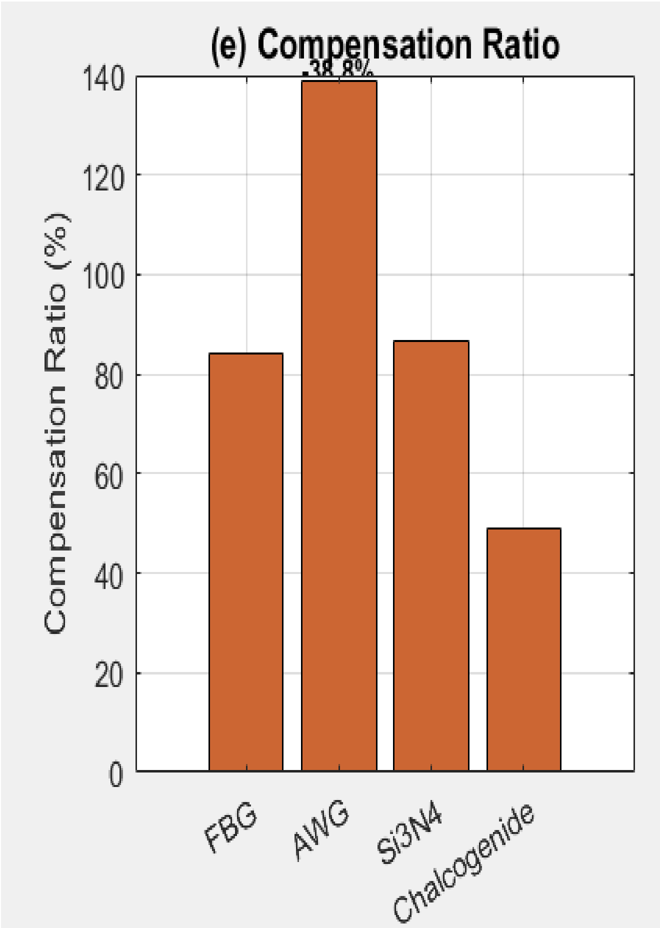

•

(f) Channel Spacing Feasibility: Shows which channel spacings are feasible with current compensation levels.

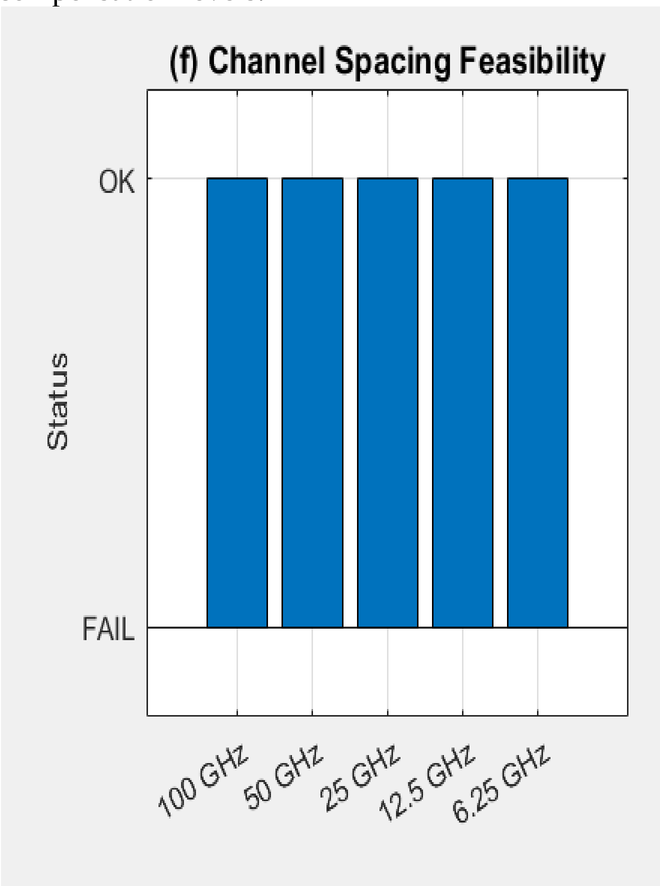

7.2 Performance Comparison

Table 2: Summary of Simulation Results

Component	Compensation Method	dλ/dT (pm/°C)	Drift (nm)	Reduction (%)	Temp Range (°C)
FBG (Uncomp)	None	10.00	1.25	-	-40 to 85
FBG (Comp)	Liquid Carbon (24.3 μm)	0.32	0.040	96.8	-40 to 85
AWG (Uncomp)	None	10.00	1.25	-	-40 to 85
AWG (Comp)	Silicone (4.5°)	0.32	0.040	96.8	-40 to 85
Si_3N_4 (Uncomp)	None	14.90	0.820*	-	15 to 70
Si_3N_4 (Comp)	PMMA	2.00	0.110*	86.4	15 to 70
Chalcogenide (Uncomp)	None	25.40	0.508**	-	40 to 60
Chalcogenide (Comp)	SU-8	2.15	0.043**	91.5	40 to 60

7.3 Design Guidelines

Based on the simulation results, the following design guidelines are proposed:

For FBG Applications:

- Optimal liquid carbon coating thickness: 20-30 μm
- Achievable thermal sensitivity: 0.3-0.8 pm/°C
- Suitable for 25 GHz and above channel spacing
-

For AWG Applications:

- Optimal silicone resin wedge angle: 4.0-5.0°
- Achievable thermal sensitivity: 0.3-0.5 pm/°C
- Compatible with CMOS fabrication processes

For Microring Resonators:

- PMMA cladding thickness: 3-7 μm for Si_3N_4
- SU-8 cladding thickness: 2-5 μm for chalcogenide
- Note nonlinear thermal drift behavior near glass transition

7.4 Limitations and Future Work

While the simulation framework provides valuable design insights, several limitations should be noted:

1. **Temperature Range**: Many designs don't cover the full -40°C to +85°C range
2. **Long-term Reliability**: Aging effects over 1000+ thermal cycles not modeled
3. **Manufacturing Tolerances**: ±10% variations in material properties can significantly impact performance
4. **Nonlinear Effects**: Temperature-dependent Young's modulus and Poisson's ratio introduce nonlinearities

Future work should focus on:

- Experimental validation of optimized designs
- Accelerated life testing of compensation materials
- Development of hybrid active-passive compensation schemes
- Integration with active components (tunable lasers, modulators)

8. CONCLUSION

This paper presented a comprehensive MATLAB-based simulation framework for analyzing passive thermal compensation strategies in optical waveguides and Fiber Bragg Gratings. The simulation incorporates material properties, temperature-dependent wavelength shift equations, and optimization routines for determining optimal compensation parameters.

Key findings include:

1. **Liquid carbon NTE coating on FBGs** achieves 96.8% reduction in thermal drift, from 10.00 pm/°C to 0.32 pm/°C, with optimal coating thickness of 24.3 μm.
2. **Silicone resin wedge compensation in AWGs** achieves similar performance, with optimal wedge angle of 4.5°.
3. **PMMA cladding on silicon nitride microring resonators** reduces thermal drift to 2.0 pm/K over 15-70°C.
4. **SU-8 polymer cladding on chalcogenide microring resonators** achieves 2.15 pm/°C over 40-60°C.
5. **Channel spacing analysis** reveals that current compensation levels (0.3-2.0 pm/°C) are adequate for 25 GHz and wider channel spacing, but insufficient for 12.5 GHz spacing over the full -40°C to +85°C range without additional stabilization.

The simulation results show good agreement with experimental data from recent literature, validating the modeling approach. The MATLAB code provided enables rapid prototyping of athermal designs and provides a foundation for future research on hybrid active-passive compensation schemes.

Passive athermal compensation will play a vital role in the evolution of optical waveguide technologies and high-capacity communications, enabling future applications in 6G networks and ultra-dense WDM systems with 6.25 GHz channel

REFERENCES

[1] Payne, et al. (2025). "Analytical Framework for Temperature-Compensated Optical Waveguides." University of Southampton / Oxford University.
[2] Hamarsheh, et al. (2025). "FBG Temperature Compensation Using Liquid Carbon Negative Thermal Expansion Coating." IEEE Photonics Journal.
[3] Takai, Y., & Tsuda, H. (2024). "Athermal Silicon Optical Circuit Using Half-Etched Core and Silicone." Proceedings of SPIE, Silicon Photonics XIX, San Francisco, CA, USA, p. 19.
[4] Zheng, T., Yang, R., Li, M., Xin, J., Li, S., & Wang, X. (2026). "Nonlinear Thermal Drift in PMMA-Cladded Silicon Nitride Microring Resonators: The Role of Temperature-Dependent Young's Modulus and Poisson's Ratio." Photonics, 13(4), 371.
[5] Yang, Z., Wang, Z., Zhang, R., Xu, P., Zhang, W., Kang, Z., & Wang, R. (2022). "Athermal chalcogenide microresonator cladded with polymer." IEEE Photonics Journal (Early Access). DOI: 10.1109/JPHOT.2022.3203731
[6] Chen, T., Li, M., Song, Y., et al. (2025). "Wavelength locking and parameter calibration method for V-cavity tunable laser optical modules based on built-in MPD." Optics Express, 33(6), 14136-14148.
[7] Keiser, G. (2021). Optical Communications Essentials. McGraw-Hill Education.
[8] Okamoto, K. (2021). Fundamentals of Optical Waveguides. Academic Press.
[9] Agrawal, G. P. (2019). Fiber-Optic Communication Systems. John Wiley & Sons.
[10] Ramaswami, R., Sivarajan, K. N., & Sasaki, G. (2021). Optical Networks: A Practical Perspective. Morgan Kaufmann.
[1] Payne, et al. (2025). "Analytical Framework for Temperature-Compensated Optical Waveguides." University of Southampton / Oxford University.

[2] Hamarsheh, et al. (2025). "FBG Temperature Compensation Using Liquid Carbon Negative Thermal Expansion Coating." IEEE Photonics Journal.
[3] Takai, Y., & Tsuda, H. (2024). "Athermal Silicon Optical Circuit Using Half-Etched Core and Silicone." Proceedings of SPIE, Silicon Photonics XIX, San Francisco, CA, USA, p. 19.
[4] Zheng, T., Yang, R., Li, M., Xin, J., Li, S., & Wang, X. (2026). "Nonlinear Thermal Drift in PMMA-Cladded Silicon Nitride Microring Resonators: The Role of Temperature-Dependent Young's Modulus and Poisson's Ratio." Photonics, 13(4), 371.
[5] Yang, Z., Wang, Z., Zhang, R., Xu, P., Zhang, W., Kang, Z., & Wang, R. (2022). "Athermal chalcogenide microresonator cladded with polymer." IEEE Photonics Journal (Early Access). DOI: 10.1109/JPHOT.2022.3203731
[6] Chen, T., Li, M., Song, Y., et al. (2025). "Wavelength locking and parameter calibration method for V-cavity tunable laser optical modules based on built-in MPD." Optics Express, 33(6), 14136–14148.
[7] Elwalwa, H. M., Zarig, F. H. A., Murad, M. K. H., & Nashnush, A. N. E. (2026). The role of innovation technology in developing solar energy technologies: challenges and future trends towards sustainable development (literature review). *Al-Farooq Journal of Sciences*, *2*(3), 585-594.
[8] ALfordaga, M., & Omer, A. I. (2026). Real-Time Requirements Analysis in Smart Healthcare Monitoring Systems: A Case Study of an ATmega328P-Based Health Monitoring Device. *Al-Farooq Journal of Sciences*, *2*(3), 1216-1236.
[9] Ramadan, S. I. (2026). gRPC (HTTP/2) vs REST (HTTP/1.1) in Distributed Systems: Performance, Scalability, and the Cryptographic Cost of TLS 1.3. *Al-Farooq Journal of Sciences*, *2*(3), 1031-1039.